Landsat-8 TIRS Thermal Radiometric Calibration Status

Julia A. Barsi* [a], Brian L. Markham [b], Matthew Montanaro [c],
Simon J. Hook [d], Nina G. Raqueno [c], Jeffrey A. Miller [e], Rasa Willette [b]
[a] SSAI, NASA/GSFC Biospheric Sciences Laboratory, Greenbelt MD, USA 20771;
[b] NASA/GSFC Biospheric Sciences Laboratory, Greenbelt MD, USA 20771;
[c] Center for Imaging Science, Rochester Institute of Technology, Rochester NY 14623;
[d] NASA/Jet Propulsion Laboratory, Pasadena, CA 21109;
[e] SGT, NASA/GSFC Biospheric Sciences Laboratory, Greenbelt, MD, USA 20771;

ABSTRACT

The Landsat-8 Thermal Infrared Sensor (TIRS) has been acquiring two-band thermal infrared images of the Earth's surface since 2013. The calibration of the two-band system has been monitored using the on-board calibrator and validated with vicarious calibration performed by NASA/JPL and RIT since launch. Soon after launch, it was discovered that the instrument had a significant stray light effect that was affecting the radiometric calibration. The stray light was corrected in the processing system in 2017. Since then, it has become apparent that there was an additional radiometric error, based on the vicarious calibration results.

With a failure within the primary electronic system and subsequent switch to the redundant electronic system, the TIRS instrument effectively has two separate calibration regimes. The vicarious calibration found a statistically significant calibration error, primarily a constant over time, in Band 11 on the primary electronics (Feb 11, 2013 through March 5, 2015) of about -0.6K at 300K. The calibration error in Band 10 was smaller though still statistically significant at about 0.2K at 300K.

On the redundant side (March 5, 2015 to present), the calibration error is more signal dependent than time dependent. Both bands are affected, with Band 10 having an error between 1K and -0.4K (between 273-320K) and Band 11 having an error between 0.8K and -1.44K (between 273-320K).

This calibration error will be corrected within the USGS Landsat Product Generation System with the release of Landsat Collection-2 products.

The Collection-2 release also includes a correction to the relative radiometric calibration of TIRS data. Striping as a result of poor detector-to-detector normalization has been increasing in the imagery since launch. The TIRS relative radiometric calibration will be updated based on internal calibrator data to remove the stripes on a quarterly basis. The visible stripes are generally at 0.1-0.2% level, though there are some detectors in each band that have changed by 1% or more. The Collection-2 release will result in much more uniform TIRS images.

Keywords: Landsat, TIRS, radiometric calibration, thermal band

1. INTRODUCTION

Landsat-8, launched in 2013, continues the long history of Landsat Earth imaging. The satellite carries two different imagers, the Operational Land Imager (OLI), which images in the visible through shortwave infrared spectral regions (0.4-2.5μm), and the Thermal Infrared Sensor (TIRS), which images in the long-wave spectral region. Though the instruments differ significantly from those aboard the previous Landsat satellites, they maintain continuity with the swath width, scene framing, radiometric and geometric accuracy and precision, and the general spectral bandwidths. Details of OLI are covered elsewhere[1,2,3]; this paper will focus strictly on TIRS.

* julia.barsi@nasa.gov; phone 1 301 614-6667

1.1 The TIRS Instrument

TIRS is the first thermal Landsat instrument to feature a pushbroom focal plane design and two spectral bands. The pushbroom focal plane consists of three separate arrays of detectors, or Sensor Chip Assemblies (SCAs), each 512 x 640 pixels, to cover the 185km swath width (Figure 1). The spectral interference filters each cover about 30 rows of each chip, though only a single row is read to generate the standard image product. The filters were designed to provide optimal band coverage for use in a split-window atmospheric correction algorithm. The spectral coverage of the two bands is shown in Figure 2.

TIRS includes on-board calibration capabilities, with a Scene Select Mechanism (SSM) that can switch the view of the telescope from the Earth to a variable temperature blackbody to deep space (Figure 3). The blackbody and deep space views are used for monitoring the internal calibration of the system. The blackbody is nominally kept at a single temperature (295K), though several times a year the blackbody is cycled through a range of temperatures. Details of the on-board calibration methods can be found in Montanaro (2014)[4].

The initial operations concept planned for acquiring images of the blackbody and deep space twice on every orbit. However, in late 2014, the encoder which detects the position of the SSM began drawing increasing levels of current, eventually reaching levels thought to threaten the operation of the SSM. After several months attempting to get the current under control, in March 2015, the instrument was switched to using the redundant electronics. The problem was believed to be a degenerative hardware issue, which might not be present in the redundant electronics. However, after several months, the redundant encoder electronics began to exhibit similar issues with current draw. In October 2015, in order to preserve the SSM encoder, standard operations of TIRS were modified to limit acquisitions that required changing the SSM position as well as turning the encoder off while operating in standard Earth imaging mode.

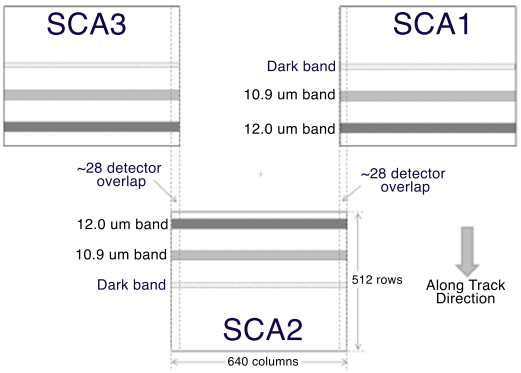

Figure 1. The TIRS focal plane layout. The center module (SCA2) is spatially offset from the other two. All three modules contain a full 2D array of imaging elements, but only two regions on each module are covered with the two spectral filters (~30 rows wide). There are about 28 detectors of overlap between the adjacent modules. The per-band images are generated from a single row from each module.

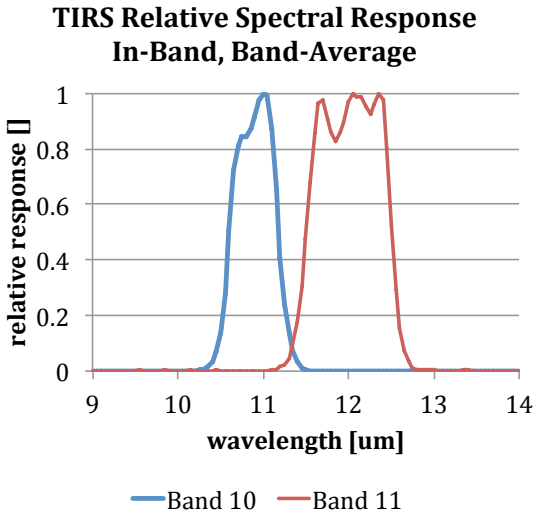

Figure 2. The band-average relative spectral responses for the two TIRS bands. The bandpasses were originally selected to optimize the use of split-window atmospheric correction techniques.

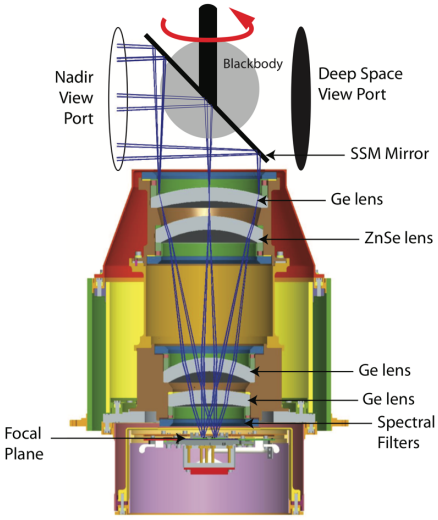

Figure 3. TIRS optical diagram. The SSM mirror rotates between the nadir viewport, blackbody and deep space viewport to provide calibration data.

Blackbody and deep space acquisitions are now performed only twice a month with the encoder powered. This acquisition change affects the radiometric calibration by not having concurrent knowledge of the background response every orbit, but due to the radiometric stability of TIRS, the loss of the encoder had a larger effect on the geometric calibration[a] [5].

Stray light was detected in the TIRS telescope in the first year on orbit. A model of the effect of the stray light on the focal plane was developed and an algorithm to remove it was implemented in the processing system in 2017[6]. All TIRS data were reprocessed using the stray light correction[7] and all data analyzed here include the correction.

2. INTERNAL CALIBRATION

The internal calibration system consists of a variable temperature blackbody, a port for viewing deep space, and the SSM, which switches the view of the telescope between the Earth view and the two calibration views. The blackbody and deep space images are acquired at the top and bottom of an orbit. The response of TIRS to the calibrators is used to monitor long-term stability of the instrument. The on-board responsivity [DN/W/m^2 sr μm] is calculated from the response of the instrument to the blackbody and deep space for individual calibration sequences.

$$g = \frac{(Q_{BB} - Q_0)}{(L_{BB} - L_{space})} \quad (1)$$

where Q_{BB} is the bias-subtracted, linearized digital counts extracted from the blackbody image, Q_0 is the instrument offset, which incorporates instrument and electronic biases, L_{BB} is the spectral radiance [W/m^2 sr μm] of the blackbody as converted from the monitor thermistor readout, and L_{space} is the spectral radiance [W/m^2 sr μm] of deep space, assuming a 4K background.

[a] Without feedback from the encoder holding the SSM in place, the SSM drifts slowly from its last controlled position to a stable location. The geometric calibration has to account for this movement in order to align the TIRS and OLI data, so new tools and models were needed. With the current operational mode, after every blackbody calibration, it takes several days for the SSM position to stabilize and for TIRS to acquire enough data to develop a model for the encoder position. The geometric registration has greater uncertainty until the data are reprocessed with an updated model of the encoder position (within several days after the blackbody acquisition).

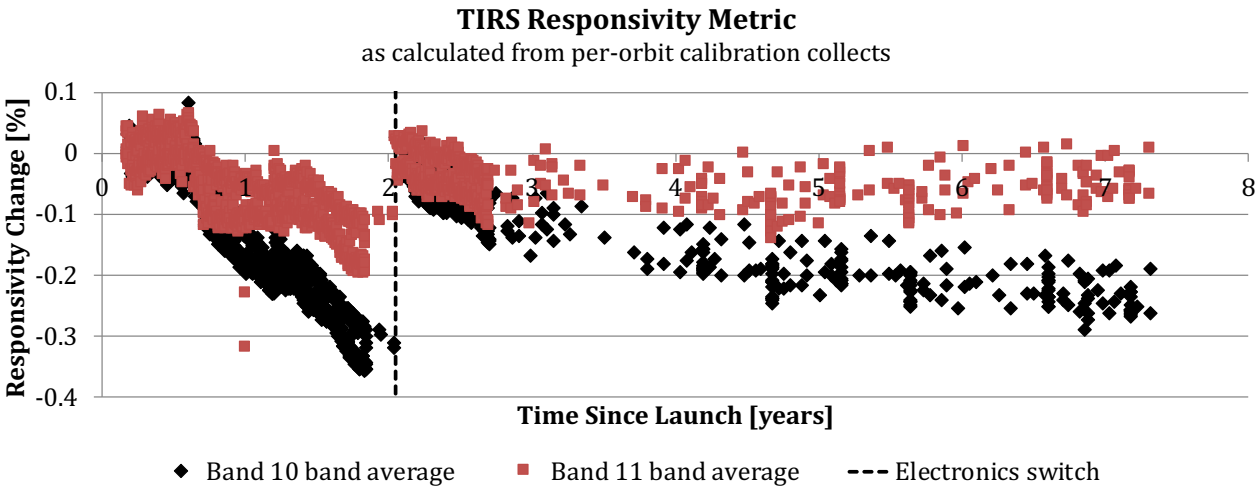

Figure 4. Long-term stability of the internal responsivity of both bands of the TIRS instrument. There was a noticeable decrease in responsivity for the first two years of the mission, but the switch to the redundant electronics slowed the effect. Note that the data are normalized separately: data acquired with the primary electronics are normalized to the first images acquired with the primary electronics and data acquired after the switch to the redundant electronics are normalized to the first images acquired with the redundant electronics.

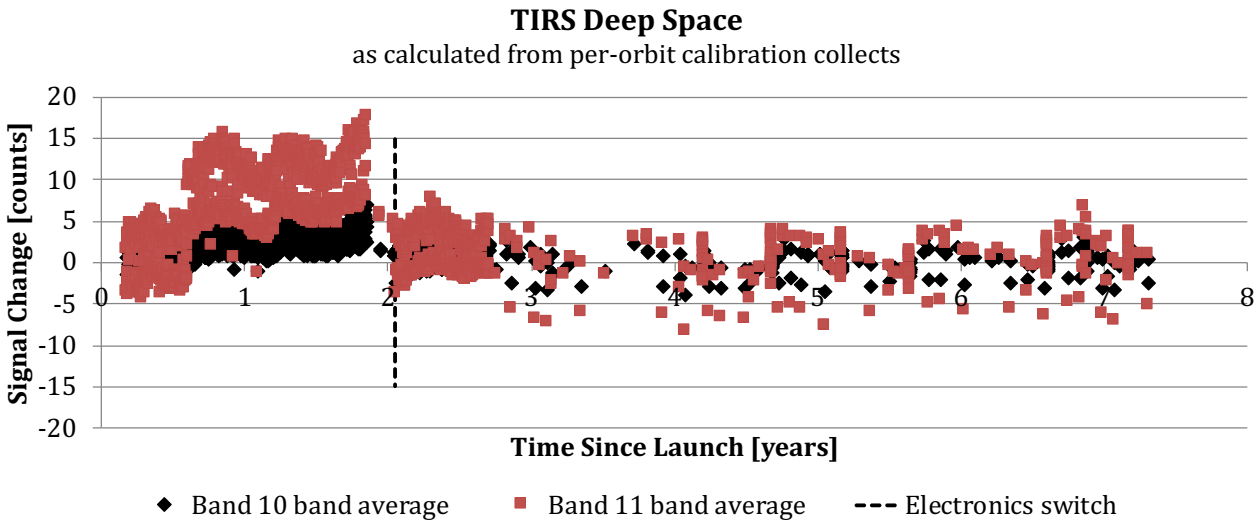

Figure 5. Long-term stability response to deep space for both bands of the TIRS instrument. The drift apparent while using primary electronics has slowed when switched to the redundant electronics.

Since launch, this responsivity metric has tracked some change over time on both electronics sides, with a notable change in behavior at the switch between the two. Figure 4 shows the lifetime trends in responsivity for the band averages, normalized to the start of each regime. With the primary electronics, there was a decrease in band-average responsivity of about 0.21% per year in Band 10, but after the switch to the redundant electronics, the rate of change slowed down to about 0.04% per year. The rate of decline was always slower in Band 11 for the primary electronics (0.09% per year). With the redundant electronics, the decrease initially followed Band 10 at 0.03% per year but after about 4 years since launch, the decline has almost stopped completely.

Figure 5 shows the response to the deep space view over time. As with the responsivity, both bands exhibited some drift over time on the primary electronics. That drift has stopped for both bands on the redundant electronics.

These metrics indicate that the TIRS instrument is stable to within 0.2% per year when looking at uniform targets. Other metrics detailed in Montanaro[4] also show both bands to be stable: over 36 minutes the background signal is stable to within 0.01 W/m^2 sr μm (1-sigma) and over 36 minutes the gain is stable to within 0.1% (1-sigma).

3. VICARIOUS CALIBRATION

The vicarious calibration of TIRS is carried out by teams at NASA/Jet Propulsion Laboratory (JPL) and Rochester Institute of Technology (RIT) using large water bodies and instrumented buoys. Water makes an ideal calibration source for the thermal bands: it is uniform in composition, has a high and known emissivity, and can exhibit low surface temperature variability over large areas. JPL built and maintains a fleet of buoys while RIT mines the data available from the NOAA National Data Buoy Center (NDBC) for suitable buoy measurements.

3.1 JPL Lake Tahoe and Salton Sea

JPL operates four instrumented buoys on Lake Tahoe on the California/Nevada border and one instrumented platform on the Salton Sea in Southern California for the purpose of thermal calibration. Lake Tahoe is situated at a high altitude, so the atmosphere is a less significant factor in thermal calibration, and the lake is extremely deep, so it never freezes. The lake has an annual temperature range from about 4C to 20C. The Salton Sea is below sea level, and the atmosphere is generally quite thick, but the water can reach temperatures up to 35C, so it extends the range of temperatures over which calibration is performed.

The instrumentation on each platform includes near surface contact thermistors, near-nadir viewing calibrated radiometers, and weather stations. Data from each buoy are acquired every two to five minutes and transmitted to JPL for processing.

Images of Lake Tahoe and Salton Sea are acquired by TIRS at every opportunity for day and night passes with nadir viewing conditions. They are also each acquired in special off-nadir requests, to increase the number of clear-sky images available for calibration. The water bodies fall in the center SCA (SCA2) during the daytime acquisitions but fall across all three SCAs in the night data due to the ability of the spacecraft to adjust the pointing angle off-nadir.

3.2 RIT and NBDC Buoys

RIT makes use of the NOAA-operated fleet of moored buoys distributed in open water around the United States. Data from these buoys are archived at the National Data Buoy Center (NDBC). To date, RIT has used buoys in the Great Lakes, the Atlantic and Pacific Oceans and the Gulf of Mexico. With the variation in location and season, the temperature ranges from about 3C to 30C. While not providing as consistent a dataset as Lake Tahoe and the Salton Sea, the sheer number of buoys available means the loss of precision due to variation in targets can be compensated for by the number of measurements.

When operational, each buoy in the network records hourly subsurface temperatures as well as weather data and archives it in the NDBC database.

The buoys are located in coastal regions of the United States and are acquired every daytime opportunity by TIRS. At least 35 buoys have been used to date. The collection of buoys is distributed across the entire focal plane in the imagery, covering all three SCAs.

3.3 Methodology

To compare the surface measurement to the radiance measured by TIRS, the surface measurement must be propagated through the atmosphere. For each of the Landsat bandpasses, the governing radiance equation can be approximated as

$$L_{TOA} = \varepsilon L_T \tau + L_u + L_d(1-\varepsilon)\tau \quad (2)$$

where L_{TOA} is the predicted sensor-reaching radiance (W/m^2 sr μm), ε is the emissivity of the target (0.995 for water), L_T is the spectral blackbody radiance associated with a target at temperature T, L_d is the spectral downwelling radiance, L_u is the spectral upwelling radiance, and τ is the transmission of the atmosphere between the target and the sensor. Provided knowledge of the atmosphere, the transmission and upwelling and downwelling radiances can be estimated using radiation

propagation code such as MODTRAN. RIT and JPL derive L_T from their source data, which requires different techniques based on whether it is a surface-leaving radiance, skin temperature or bulk temperature measurement. The atmospheric data are generally derived from assimilated atmospheric profile products, but in some cases, local weather data are used.

This technique was used to detect the initial error in TIRS after launch[8] and to validate the effect of the stray light correction once applied in 2017[9]. The residual calibration error after the stray light correction was reduced from several degrees to 0.3K, but the uncertainty was still larger than desired, particularly in Band 11 at 0.84K.

JPL and RIT continue to collect vicarious calibration data for TIRS. The additional several years of data since 2017 has been included into the analysis reported here.

Table 1. Estimates of residual errors in the vicarious calibration data once the stray light correction was applied[9]. While the absolute errors were reduced with the stray light correction, the larger than desired uncertainties suggested that more assessment was needed.

Band	Number of Acquisitions	Calibration Error [W/m^2 sr µm]	Calibration Error [K at 300K]	Uncertainty [K]
Band 10	368	-0.04	-0.30	0.51
Band 11	368	0.04	0.29	0.84

4. ABSOLUTE CALIBRATION ANALYSIS

The sensor-reaching radiances predicted from the surface measurements are compared directly to the stray light corrected radiance measured by TIRS for both bands (Figure 6). The residual differences between the radiances are analyzed for patterns and trends to detect remaining calibration errors.

In the lifetime analysis of the stray light corrected data, data acquired at night are separated from data acquired during the day. Since there is no solar loading at night, imaging conditions are generally more stable, and the uncertainty is lower. The night data here are used to help establish trends. However, since more than 99% of TIRS data are acquired during the day, the daytime results are used for establishing corrections to the calibration.

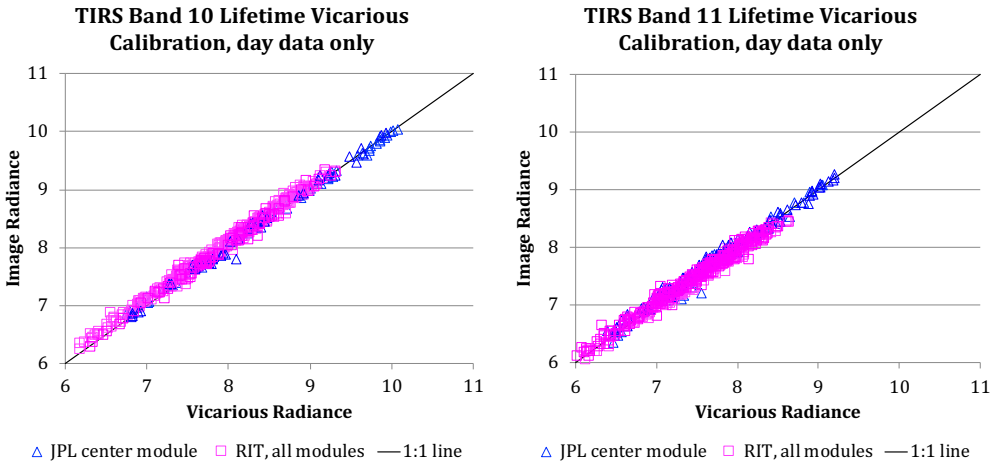

Figure 6. Lifetime vicarious calibration for the daytime data from both JPL and RIT. The sensor-reaching radiance predicted by the surface measurements are compared directly to the radiances derived from the TIRS response. The intent is that the data all fall on the 1:1 line.

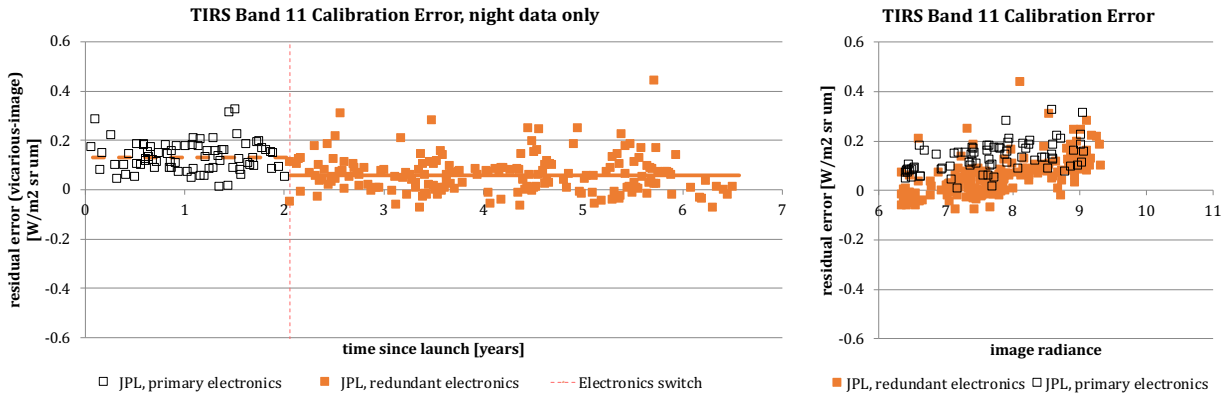

Figure 7. Lifetime residual calibration error over time for Band 11, nighttime data (JPL only). The calibration error is different for the two sets of electronics. The time-dependent error is shown on the left and the signal-dependent is shown on the right and both are statistically significant.

4.1 Nighttime Calibration Results

As was reported in 2017[9], there was a hint of a calibration difference between the primary and redundant electronics sides. It was most clear in the nighttime data (Figure 7), though the difference was also statistically significant in the day data. With further analysis, the difference between the calibrations on the two electronics systems was concluded to be real. With the current data set, if considered as a bias-only error, for Band 11 the residual error on the primary electronics side is 0.13±0.01 W/m^2 sr μm while it is 0.06±0.01 on the redundant side. However, there is also statistically significant error that is dependent on signal level. For Band 11, data on both electronics sides exhibit a signal-dependent calibration error. These results were not used to generate the final calibration update, but they guided decision making on what was significant.

4.2 Daytime Calibration Results

Figure 6 shows the vicarious calibration results in radiance for daytime data for both bands for the lifetime without distinguishing between the two electronics sides. The data are scattered about the 1:1 line at this scale, though a closer look reveals both gain and offset errors.

The residual errors are plotted over time in Figure 8 for daytime data, with a summary provided in Table 2. The Band 10 data show good agreement between the RIT and JPL data with little seasonal variability apparent. The difference between the data acquired on the primary and redundant sides is statistically significant. The Band 11 data are more scattered than Band 10 and the two teams' datasets show less agreement. In both bands, there is a residual bias error that is statistically significant though much smaller than the early performance before the stray light correction. Figure 9 shows the error over signal level for Band 11. On the primary side for Band 11, there does not appear to be a dependence on signal level in either dataset and that is reflected in a nearly horizontal fit to the data (black dashed line). However, on the redundant side, the residual errors are signal dependent and the fit has ~5% slope to it. The pattern for Band 10 calibration error is similar, with very little signal-dependent error on the primary side, but a ~3% signal dependence on the redundant side.

Because the JPL daytime data are acquired within a single SCA but the RIT data are acquired across all SCAs, the difference between the calibration of individual SCAs was checked. When splitting the data by SCA and performing the same analysis for each SCA separately, the differences between the SCAs are not statistically significant. The calibration errors do not appear to be related to calibration differences between the SCAs, as far as can be determined from the RIT and JPL dataset.

Figure 8. Lifetime residual calibration error over time for both bands. The calibration error changes at the switch between electronics side.

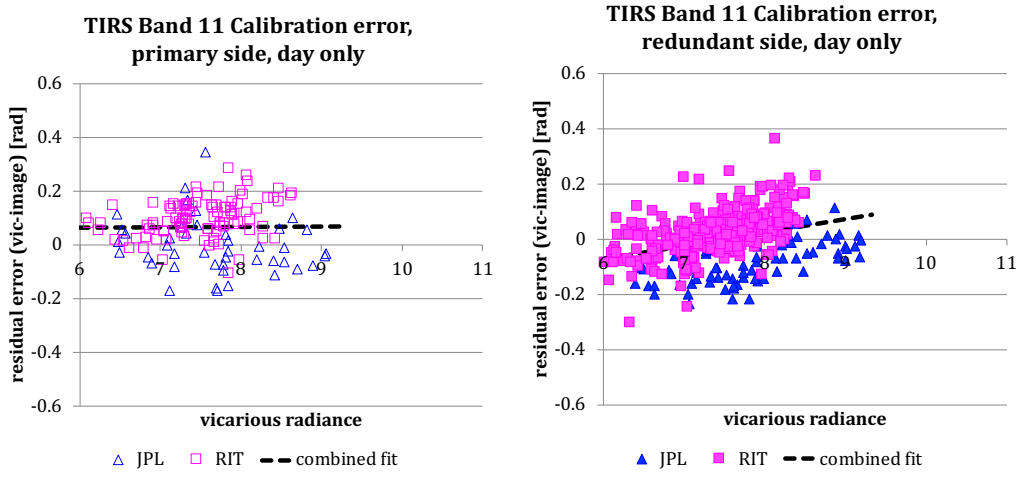

Figure 9. Lifetime residual calibration error over radiance level for Band 11. The two data sources, JPL and RIT, don't agree as well in Band 11 as they do in Band 10, which is likely due to a residual stray light error. The error on the primary electronics side is primarily a bias error, but on the redundant side, it is a gain error. The combined residual error is shown as the black line.

Table 2. Current estimates of TIRS Collection-1 calibration errors for the combined RIT and JPL daytime dataset for the two electronics side time periods separately.

Band	Electronics	Number of Acquisitions	Gain Error [unitless]	Period Average Bias Error [W/m^2 sr µm]	Estimated Calibration Error at 300K [K]
Band 10	Primary	142	1.01 ± 0.02	-0.02	-0.20
	Redundant	368	0.97 ± 0.01	-0.06	-0.12
Band 11	Primary	142	1.00 ± 0.03	0.07	0.56
	Redundant	368	0.95 ± 0.01	0.00	0.58

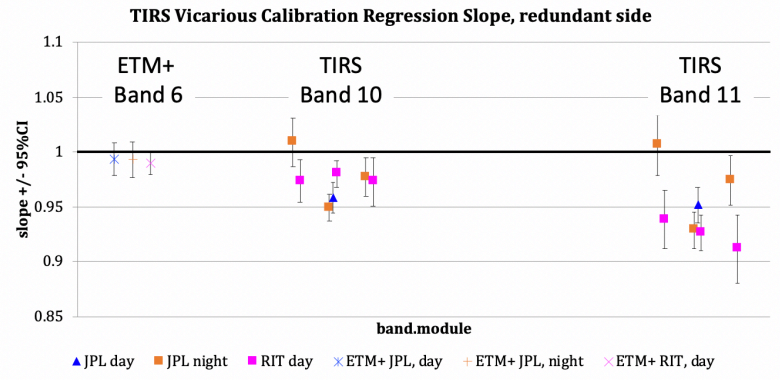

Figure 10. Comparison of calibration error slope for the TIRS bands, split by module, and the ETM+ thermal band over the same time period. The ETM+ results do not indicate a gain error, since they are not statistically different than 1. Since the instruments do not agree, the likely source of error is not the vicarious methodology or surface measurement data.

There are also Landsat-7 ETM+ vicarious calibration data for this time period for the same collection of sites. The slopes and biases of the ETM+ residual calibration errors do not indicate change similar to this over the lifetime of Landsat-8, ruling out changes in the targets over the time period. The ETM+ vicarious calibration data since 2013 continue to suggest that the ETM+ thermal band is calibrated to within 0.4K[10], with no statistically significant signal-dependent error. Figure 10 illustrates the slopes of the vicarious calibration results broken down by SCA along with the ETM+ slopes for the same time periods.

4.3 Collection-2 Calibration update

New calibration coefficients were determined based on the errors in Table 2. An analytical model of the update was used to verify that the new parameters would have the desired effect on the entire RIT and JPL dataset. Then a randomly selected 25% of the RIT and JPL data were reprocessed with the new calibration coefficients to verify the processing system also produced the desired results. The analytical results and image reprocessed radiance agreed to the expected levels. Figures 11 and 12 show the residual calibration error after the calibration was updated. As expected, there is no statistically significant residual calibration error. The statistics on the residual errors are in Table 3.

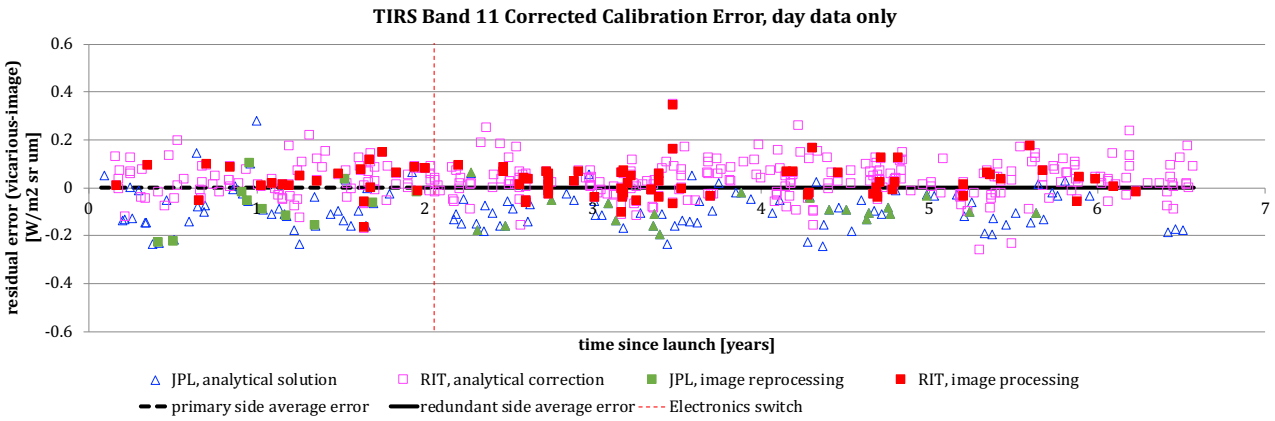

Figure 11. Lifetime residual calibration error over time for Band 11 after the calibration correction is applied. The correction was made to all data analytically, but only 25% of the scenes were reprocessed through the image processing system. The reprocessed results agree with the analytical results. The combined analytical dataset has no residual calibration bias on either electronics side.

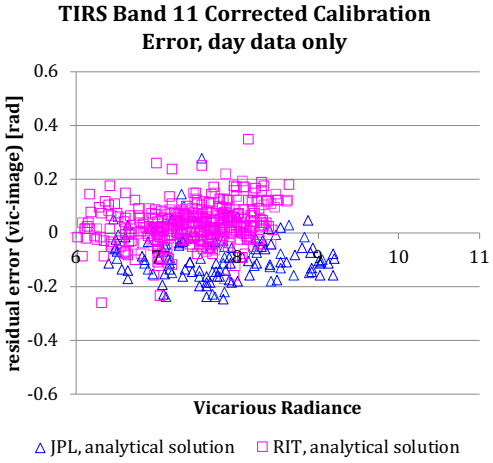

Figure 12. Lifetime residual calibration error over signal level for Band 11 after the calibration correction is applied. The combined analytical dataset has no residual calibration gain on either electronics side.

Table 3. Collection-2 predicted results for the combined JPL and RIT dataset.

Band	Electronics	Number of Acquisitions	Calibration Error [W/m^2 sr µm]	Calibration Error [K at 300K]	Uncertainty [K]
Band 10	Primary	142	0.00 ± 0.01	0.0	0.51
	Redundant	329	0.00 ± 0.01	0.0	0.41
Band 11	Primary	142	0.00 ± 0.02	0.0	0.76
	Redundant	329	0.00 ± 0.01	0.0	0.73

Table 4. The estimated change in response as a result of the calibration update for both TIRS bands at a range of temperatures for both electronics sides[12]. The error is significantly more signal dependent on the redundant side. Positive errors indicate the Collection-1 response was too hot, negative errors indicate the Collection-1 response is too cold. The estimates at 240 and 320K are extrapolated outside of the temperature range over which the calibration was derived.

Temperature [K]	TIRS Band 10 Change in Response [K]		TIRS Band 11 Change in Response [K]	
	Feb 11, 2013 - Mar 1, 2015 primary side	Mar 2, 2015 – present redundant side	Feb 11, 2013 - Mar 1, 2015 primary side	Mar 2, 2015 – present redundant side
240 (extrapolated)	-0.11	2.73	-0.89	3.16
273	0.08	1.05	-0.66	0.80
285	0.14	0.60	-0.61	0.15
300	0.20	0.12	-0.56	-0.58
320 (extrapolated)	0.27	-0.42	-0.51	-1.44

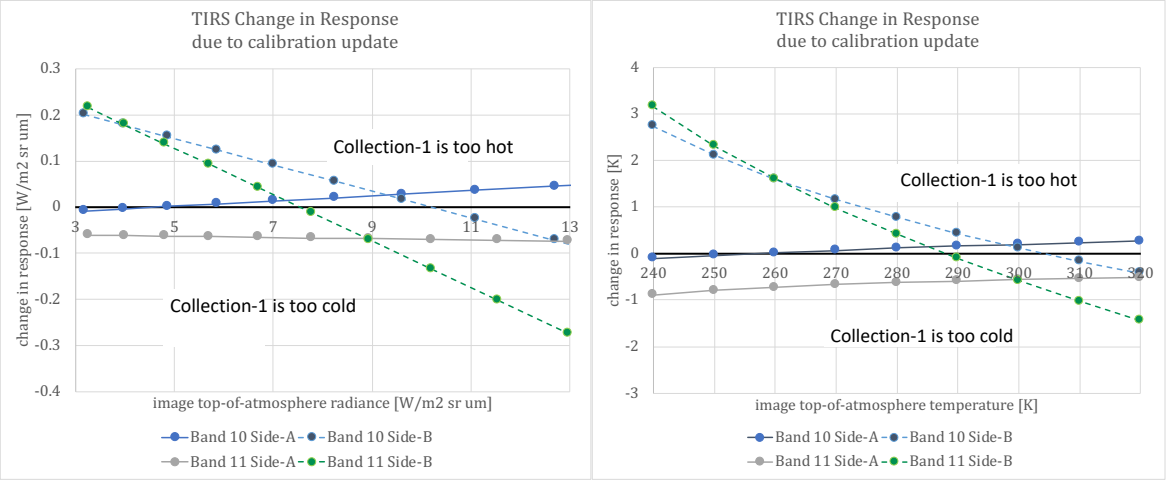

Figure 13. The estimated change in response as a result of the calibration update for both TIRS bands for both radiance and temperature.[12]

Based on these results, the absolute calibration of both TIRS bands will be updated in the USGS Landsat Product Generation System to Collection-2 in 2020[11]. The change will affect the images acquired on the two electronics sides differently and will be signal dependent. Table 4 and Figure 13 provide an estimate of the changes expected for specific target temperatures.

5. RELATIVE CALIBRATION

With 1920 individual detectors per band across the TIRS focal plane, the relative calibration of the instrument is important to minimize detector-to-detector differences that cause stripes in the image data. The prelaunch characterization of the relative gains was generated based on a collection of blackbody data acquired while TIRS was in a thermal vacuum chamber. The instrument was looking at a uniform wide-aperture blackbody source that filled the TIRS field of view and images were acquired at a range of temperatures between 200 and 360K. These data were used to characterize the linearity, absolute responsivity and relative response for both bands and on both electronics sides. Once on-orbit, the primary side relative gains were modified to account for contamination that appeared on the Band 11 filter sometime between the last prelaunch measurement and on-orbit activation[4]. When the electronics side changed on 2015, the relative gains were updated, as well as all of the other radiometric calibration parameters, to the values established during pre-launch testing of the redundant side.

5.1 Characterization of on-orbit performance

Except for the two modifications, the TIRS relative gains have remained unchanged, even though striping in the imagery has appeared to get worse (Figure 14). A study based on images of very uniform cloud-free regions of open ocean established that the streaking in Level-1 radiance products was increasing over time in both bands. Streaking (s_i) is a metric to quantify the difference between adjacent detectors in the image data:

$$s_i = L_i - 0.5\left[\frac{L_{i-1} + L_{i+1}}{\bar{L}}\right]$$

where L is the per-detector average radiance from the image subset, $\bar{L}$ is the average radiance across the array, and i is the detector index. Over uniform targets, the streaking is a measure of nonuniformity of the image product (Figure 15). The standard deviation of the per-detector streaking metric provides an overall estimate of the nonuniformity across the focal plane. Tracking the standard deviation of the streaking metric for each image over time provides a quantitative estimate of the state of the in streaking and thus, the effectiveness of the relative gains to flatfield the image data. Figure 16 shows the standard deviation of the streaking over time for a series of cloud-free open ocean image subsets. This study shows that streaking was increasing over time and the relative gains appeared to need updating from the prelaunch estimates.

5.2 Blackbody-derived relative gains

The most uniform target available to TIRS is the internal blackbody so further studies of relative calibration proceeded using the TIRS images of the blackbody rather than images of open ocean. The TIRS blackbody is not a completely uniform source, though prelaunch characterization established the general shape of the nonuniformity. The uniformity factors are the generated from the per-detector average of TIRS images of the internal blackbody over multiple acquisitions at multiple temperatures. The per-detector radiances were normalized per image and then averaged across all temperatures. The nonuniformity factors are shown in Figure 17 for both bands and electronics sides. When applied to the blackbody images, they remove the nonuniform structure of the blackbody from the images. The residual detector-to-detector differences are the effect of the TIRS instrument.

The relative gains can now be derived based on a uniform blackbody source. For an individual TIRS image of the blackbody, the relative gains (r_i) are

$$r_i = \frac{s_i}{\bar{s} * \eta_i}$$

Where S_i is the linearized, dark-subtracted response of detector i, $\bar{S}$ is the average linearized, dark-subtracted response across all detectors and η_i is the per-detector nonuniformity factor.

The relative gains are calculated for every acquisition of the blackbody on orbit. They are averaged on a quarterly basis for application in the calibration parameter file for use in the processing system.

When it happens, general, the responsivity of individual detectors changes suddenly, all at once, and they stay at that new responsivity level. Most detectors that have changed over the TIRS lifetime have changed by less than 0.5%. There have been 13 detectors in Band 10 and 29 detectors in Band 11 that have changed by more than 0.5%. The largest individual detector change was one Band 11 detector whose responsivity dropped by 2% This method of updating the relative gains quarterly will enable the processing system to correct for new changes in detectors.

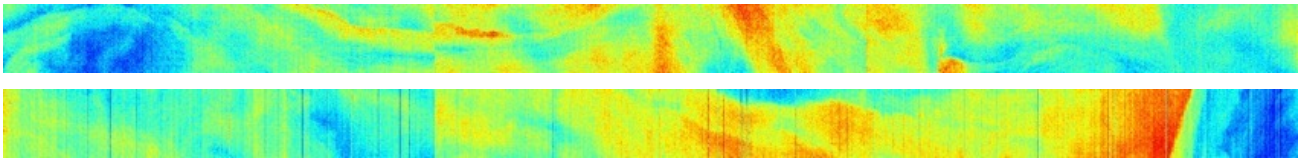

Figure 14. 100-frame striping example for two very uniform regions of open ocean in Band 10: top is from March 2013 and bottom is from August 2014. With this very extreme stretch, the small contours in the water currents are visible, as well as the change in the striping pattern. There were no apparent stripes just after launch but by mid-2014, stripes are apparent with magnitudes of between 0.2 and 0.5%.

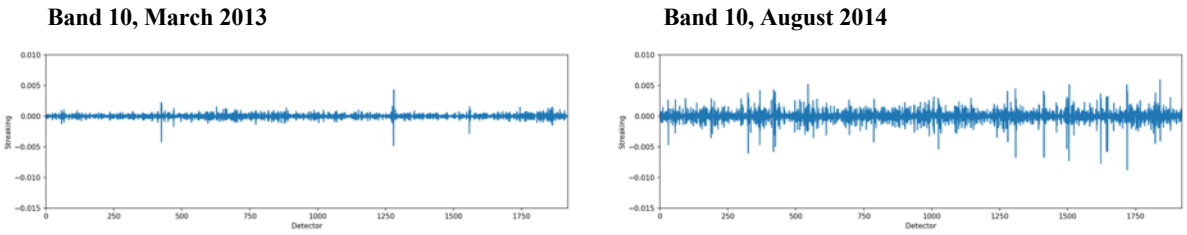

Figure 15. The per-detector streaking metric for the Band 10 open ocean images in Figure 14. The left plot is from relatively soon after launch, when the prelaunch relative gains were effective at flat fielding the images. The right plot is from the third quarter of 2014, when visible stripes were apparent in the image.

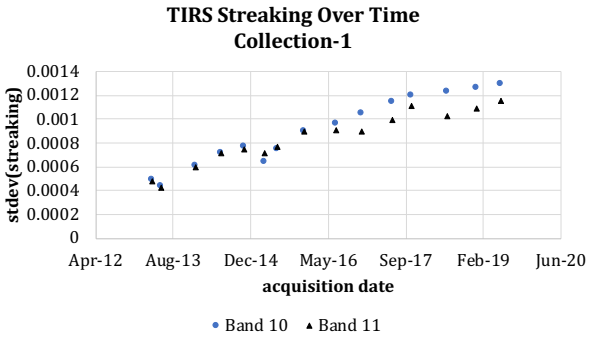

Figure 16. The standard deviation of the streaking metric over time for the cloud-free open ocean image subsets for both bands. In both bands, the streaking gets steadily worse over time, leading to more visible stripes in the images, as indicated in Figure 14 (however, the samples from Figure 14 are not included on this plot).

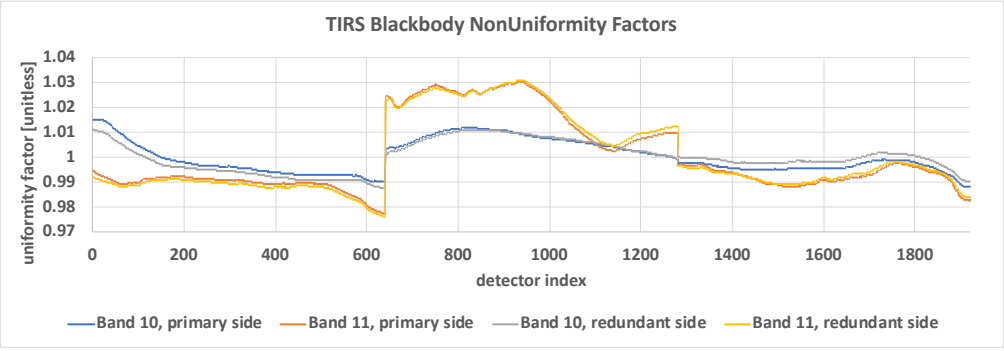

Figure 17. The nonuniformity characterization of the TIRS on-board blackbody for both bands and electronic sides. These factors can be used to flatten all TIRS blackbody images.

5.3 Improved Relative Gains

Switching from using what is effectively the prelaunch relative calibration to a per-quarter estimate derived from the internal blackbody will make a dramatic improvement in the detector-to-detector calibration. Individual detectors' responsivities have changed by as much as 2% in the worst case and there has been no accounting for that in the image products as of yet.

The streaking metric study was repeated on the same set of ocean scenes after having been reprocessed with the blackbody-derived relative gains. Results show that the new relative gains eliminate the increase of the streaking over time (Figure 18). The new current level of streaking matches the streaking in the earliest imagery, where the prelaunch gains produced a stripe-free image. An example of the reduction in striping in Band 10 is shown in Figure 19 and Band 11 is shown in Figure 20. These figures show the effectiveness of using the blackbody to estimate per-detector relative gain.

The new relative gains will be implemented in the calibration parameter file with the release of Collection-2.

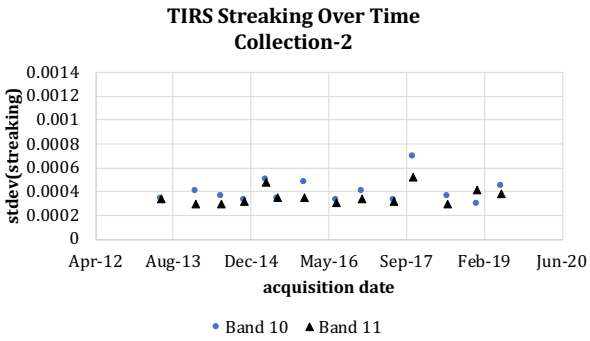

Figure 18. The standard deviation of the streaking metric over time for the cloud-free open ocean image subsets for both bands processed with the blackbody-derived relative gains. The streaking has been reduced to the baseline level established just after launch. These results can be compared directly to Figure 16 to see the statistical improvement in the reduction of streaks.

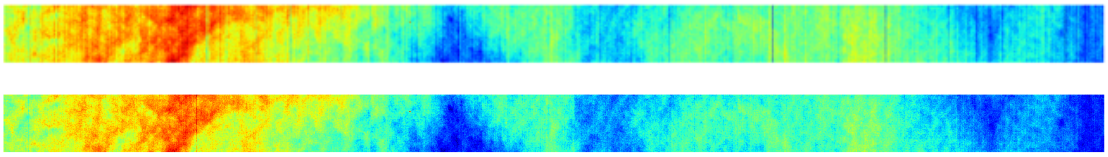

Figure 19. Visual improvement of a 100-frame sample of a Band 10 scene from the fourth quarter of 2018. The image at the top is a subset of a cloud-free open ocean image processed with the prelaunch relative gains; vertical stripes are indicative of the poor detector-to-detector normalization of the prelaunch relative gains. The bottom image is the same Band 11 image subset but processed with the blackbody-derived relative gains; the image is largely stripe-free.

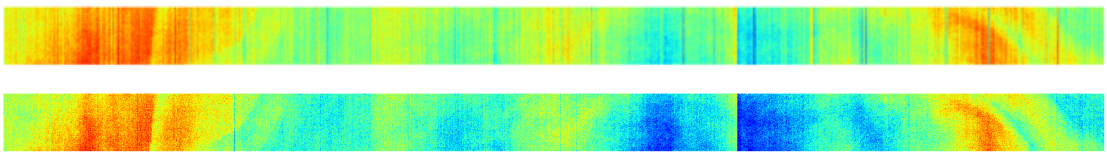

Figure 20. Visual improvement of a 100-frame sample of a Band 11 scene from the second quarter of 2018. The image at the top is a subset of a cloud-free open ocean image processed with the prelaunch relative gains; vertical stripes are indicative of the poor detector-to-detector normalization of the prelaunch relative gains. The bottom image is the same Band 11 image subset but processed with the blackbody-derived relative gains; the image is largely stripe-free.

6. CONCLUSIONS

The TIRS instrument has proven to be internally stable, particularly after the instrument was switched to the redundant electronic system in 2015. The internal blackbody data indicate a degradation of 0.21% in responsivity on the primary electronic system but the trend flattened on the redundant electronics system. Since 2017, the slow decrease in responsivity, as represented by the internal calibration system, has stabilized.

Since the stray light correction was implemented in 2017, the vicarious calibration effort has continued to validate the absolute calibration of TIRS. The data indicate that TIRS has both time and signal dependent calibration errors in both bands. The errors did not appear to be dependent on SCA and similar errors were not detected in the Landsat-7 ETM+ data over the same time period. The vicarious calibration data were used to generate new calibration parameters which will be implemented in the Colletion-2 processing system. The new products will be calibrated to within 0.5K in Band 10 and 0.75K in Band 11.

A study of striping in TIRS image data revealed that striping was getting worse over time. The prelaunch relative gains will be replaced in the Collection-2 processing system, significantly improving the appearance of TIRS data for the whole mission.

The Collection-2 update includes some very significant for changes for the TIRS bands. Every image will be affected by both the absolute and relative calibration updates. Users should replace their Collection-1 data with the Collection-2 data in their long-term studies.

REFERENCES

[1] Markham, B.L., Barsi, J.A., Kvaran, G. Ong, L., Kaita, E., Czapla-Myers, J., Mishra, N., Helder, D.L. "Landsat-8 Operational Land Imager Radiometric Calibration and Stability," Remote Sensing 6(12), 11753-11769 (2014).

[2] Morfitt, R., Barsi, J.A., Levy, R. Markham, B.L., Micijevic, E., Ong, L., Scarmuzza, P., Vanderwerff, K. "Landsat-8 Operational Land Imager Radiometric Performance On-Orbit," Remote Sensing 7(2), 2208-2237 (2015).

[3] Brian Markham, Julia Barsi, Matthew Montanaro, Joel McCorkel, Aaron Gerace, Jeffrey Pedelty, Simon Hook, Nina Raqueno, Cody Anderson, Md Obaidul Haque, "Landsat-8 on-orbit and Landsat-9 pre-launch sensor radiometric characterization," Proc. SPIE 10781, Earth Observing Missions and Sensors: Development, Implementation, and Characterization V, 1078104 (23 October 2018); https://doi.org/10.1117/12.2324715

[4] Montanaro, M., Levy, R., and Markham, B. "On-orbit radiometric performance of the Landsat 8 Thermal Infrared Sensor," Remote Sensing 6(12), 11753-11769 (2014).

[5] Storey, J.C. personal communication (2017).

[6] Gerace, A., and Montanaro, M. "Derivation and validation of the stray light correction algorithm for the thermal infrared sensor onboard Landsat 8," Remote Sensing of Environment 191, 246-257 (2017).

[7] USGS, "TIRS Stray Light Correction Implemented in Collection 1 Processing,", 25 April 2017, https://landsat.usgs.gov/april-25-2017-tirs-stray-light-correction-implemented-collection-1-processing (accessed 18 July 2017).

[8] Barsi, J.A., Schott, J.R., Hook, S.J., Raqueno, N.G., Markham, B.L., and Radocinski, R.G., "Landsat-8 Thermal Infrared Sensor (TIRS) Vicarious Radiometric Calibration," Remote Sensing 6(11), 11607-11626 (2014).

[9] Julia A. Barsi, Brian L. Markham, Matthew Montanaro, Aaron Gerace, Simon J. Hook, John R. Schott, Nina G. Raqueno, Ron Morfitt, "Landsat-8 TIRS thermal radiometric calibration status," Proc. SPIE 10402, Earth Observing Systems XXII, 104021G (5 September 2017);https://doi.org/10.1117/12.2276045

[10] Schott, J.R., Hook, S.J., Barsi, J.A., Markham, B.L., Miller, J., Padula, F.P., Raqueno, N.G., "Thermal infrared radiometric calibration of the entire Landsat 4, 5, and 7 archive (1982-2010)," Remote Sensing of Environment 122, 41-49 (2012).

[11] USGS, "Landsat Collection 2 Level-1 Data", 15 December 2019, https://www.usgs.gov/core-science-systems/nli/landsat/landsat-collection-2 (accessed 9 August 2020)

[12] USGS, "Dec 15, 2019 – TIRS Absolute Radiometric Calibration Update", 15 December 2019, https://www.usgs.gov/land-resources/nli/landsat/landsat-8-oli-and-tirs-calibration-notices (accessed 9 August 2020).